Proceedings of ASME Turbo Expo 2014: Turbine Technical Conference and Exposition
GT2014
June 16-20, 2014, Düsseldorf, Germany

GT2014-26874

ADVANCED FLUTTER ANALYSIS OF A LONG SHROUDED STEAM TURBINE BLADE

Paul Petrie-Repar *
RPMTurbo
Ashgrove QLD 4060
Australia
Email: paul.petrie-repar@rpmturbo.com

Vasily Makhnov
LMZ Power Machines
St Petersburg
Russia

Prof. Nikolay Shabrov, Prof. Evgueni Smirnov, Sergey Galaev, Kirill Eliseev
St Petersburg State Polytechnical University
St Petersburg
Russia

ABSTRACT

An advanced flutter analysis of a final stage turbine row with a new 1.2 meter long shrouded blade is presented. The three-dimensional (3D) unsteady Reynolds Averaged Navier-Stokes (URANS) equations with the Spalart and Allmaras turbulence model were employed to model the flow. The flow entering the last stage is a mixture of saturated vapor and liquid. An equilibrium wet-steam equation of state was used to model the properties of the mixture. Multi-row steady state simulations of the upstream stator row, the turbine row and the extended exhaust section were performed. It was considered important to include the exhaust section in the steady-state simulations in order to accurately predict the pressure profile at the exit of the turbine. The flow simulations were relatively high resolution and the single passage turbine mesh had 798 208 cells. Linearized flow simulations for the turbine row were performed to determine the unsteady aerodynamic work on the blades for the possible aeroelastic modes. An exact 3D non-reflecting boundary condition (3D-NRBC) was applied at the inlet and outlet for the linearized flow simulations to eliminate non-physical reflections at these boundaries. The calculated logarithmic decrement values for the new turbine blade are compared with a reference case for a similar steam turbine blade at a condition known to have a long and safe working history. The new last stage was found to be more stable than the reference case at the flow condition examined.

*Address all correspondence to this author.

NOMENCLATURE

n Nodal diameter

INTRODUCTION

Flutter is the self excited vibration of a structure due to the interaction of aerodynamic and structural-dynamic forces. The turbine blades of the last stage of large scale industrial steam turbines are typically over one meter long. These long blades are susceptible to flutter because of their low structural frequency and supersonic tip speeds. Although no steam turbine blade failure (loss of blade) due to flutter has been reported in the literature [1], blade flutter is a concern for the manufacturers of steam turbines [1, 2] and blade root cracking at the last stage of a steam turbine due to flutter has been reported [3].

It is important that the flutter stability of at least the last stage is assessed for any new blade design or new operating condition of a large scale steam turbine. In order to analyze flutter, the coupled aerodynamic and structural dynamic (aeroelastic) system must be considered. An aeroelastic system can only be considered flutter free if all possible eigenmodes of the aeroelastic system are stable. The aeroelastic eigenmodes of a turbomachinery row are the traveling wave modes if the following assumptions are made: each blade is identical (tuned blades), unsteady aerodynamic forces do not alter the structural deformation or frequency, each blade has only one degree of freedom (DOF), unsteady flow perturbations are linear with blade vibrations and the aerodynamic (and/or structural) coupling between blades is symmetric. The traveling wave modes are patterns of blade motion

Copyright © 2014 by RPMTurbo & LMZ Power Machines

with the blades moving with a constant amplitude and with a constant phase shift between adjacent blades. This phase shift is referred to as the inter-blade phase angle and is equal to

$$\sigma_n = \frac{2\pi n}{N}, \tag{1}$$

where n is the nodal diameter and N is the number of blades in the row. A positive nodal diameter indicates that the direction of the phase (and the perceived direction of travel) of the blade vibrations of the row is in the same direction as the rotation of the rotor.

A turbine row can only be considered flutter free if all possible traveling wave modes are stable. The stability of a traveling wave mode can be determined by calculating the unsteady flow response to the blade motion of the traveling wave mode. The unsteady flow calculation can be performed on a single passage mesh if a phase shift corresponding to the inter-blade phase angle is applied to the unsteady flow perturbations at the periodic boundaries. The work (W_{aero}) performed by the unsteady flow on the blade can be calculated by integrating the unsteady pressure with the mode shape displacement. If this work is positive, the unsteady aerodynamics are adding energy to the motion of the blades.

The aeroelastic stability of each traveling wave mode is usually expressed as the logarithmic decrement of the mode which is the rate of decrease in the amplitude of the blade motion per cycle and can be calculated as

$$\delta = \frac{-W_{\text{aero}}}{2\,KE_{\max}} \tag{2}$$

where $KE_{\max}$ is the maximum kinetic energy of the blade mode shape. Note that negative values of logarithmic decrement are unstable.

If the logarithmic decrement value is negative then the level of the unsteady aerodynamic work needs to be compared with the level of structural damping. The level of structural damping will depend on the material of the blade, the blade connections and the nodal diameter. If the mechanical damping is not sufficient to overcome the positive aerodynamic work then a flutter risk exists.

The results of three-dimensional unsteady flow calculations performed for the purpose of flutter analysis of steam turbine blades have been presented previously. These methods solved the inviscid flow equations [1, 3, 4] and the URANS flow equations [2] in the time domain.

LMZ STEAM TURBINES

At the end of the 1970s, LMZ (now part of *Power Machines* company) produced steam turbines rated at 1200 MW which at that time was the record for unity power for full-speed turbines. LMZ has developed and introduced a titanium 1200mm blade at the last stage for this series of machines. In accordance with LMZ design traditions, the blade has an integral tip cover which provides a coupled system with cyclic symmetry. Shroud blades have the advantage of reducing tip leakage and increasing row stiffness [1] and mechanical damping.

For decades, the blades with small upgrades ran successfully in turbines of various ratings, including nuclear units rated at 1000 MW. These blades never failed, and the only feature of its operation in some units, was minor wearing of the contact zones in the covers of some blades that occasionally required repair during overhauls.

In the 2000s, LMZ developed and installed a system for online blade vibration control. It was observed that in some units at nominal operating conditions, regular vibrations at specific frequencies occasionally occurred. These vibrations corresponded to the first group of modes at backward-running nodal diameters. These vibrations were identified as flutter. The amplitudes of these vibrations were far from a dangerous level and posed no threat to the structural integrity of the blades due to the high mechanical damping of the blades. The only consequence of this phenomenon was the wearing of the contact zones in some tip covers. Considering a new range of possible flow conditions through the last stage it was decided to develop a flutter criteria.

In 2007, LMZ began a cooperation with RPMTurbo for the purpose of developing a flutter criteria for new operating conditions. The initial project was a *blind* test. RPMTurbo was provided with the set of nine *operating conditions* with different mass and volume flow rates. Some of the operating conditions corresponded to real working machines and the field data were not disclosed to RPMTurbo. RPMTurbo performed linearized unsteady flow simulations to calculate the logarithmic decrement of the aeroelastic modes for the nine operating conditions. The results of the flutter analysis agreed with the field data. The most valuable result of the analysis was a favorable prediction for one of the new operating conditions. The new operating condition had mass flow and back pressure values that significantly exceeded previous levels for this blade. The prediction for the new operating condition was considered to be favorable because the logarithmic decrement values were higher (more stable) than those predicted for operating conditions from real machines that already have a proven safe working history.

SCOPE OF PAPER

Recently, LMZ designed a new series of steam turbines. In this paper, the results from a flutter analysis of the new last stage shrouded blade (Fig. 1) are presented. The flutter results are compared with a reference blade. The design of the last stage was focused on providing a greater turbine exhaust area which makes it possible to reduce the overall axial length of the turbine.

Copyright © 2014 by RPMTurbo & LMZ Power Machines

The exhaust area of the reference blade was 11.3 m^2 and the flow rate was approximately 400 tonnes/hr. The new blade (stage) was developed in order to further increase the exhaust flow capacity and improve aerodynamic performance. The new blade is longer and the root diameter is larger than the reference blade. The new blade is made of steel while the reference blade is made of titanium.

Multi-row steady-state simulations of the nozzle (vane/stator) row, turbine row and exhaust section were performed. The multi-row steady-state simulations were considered necessary to accurately predict the flow conditions at the exit of the turbine because the flow at the exit was expected to be supersonic. The unsteady flow responses to the possible aeroelastic modes were calculated by a three-dimensional linearized flow solver [5]. Linear flow analysis can be used to accurately predict the unsteady flow when a single time frequency dominates and the flow perturbations are small. This assumption is valid for flutter analysis because the flow perturbations at the flutter frequency are small at the onset of flutter. Inviscid and URANS flow simulations were performed. A three-dimensional non-reflecting boundary condition (3D-NRBC) was applied at the inlet and outlet of the turbine for the unsteady flow simulations and a wet steam equation of state was also used. As far as the authors are aware, this is the first time either a wet-steam equation of state or a 3D-NRBC has been applied to a flutter analysis of an industrial steam turbine. The logarithmic decrement values for the blade are presented and normalized by the magnitude of the minimum logarithmic decrement value from an operating condition with a known safe working history.

COMPUTATIONAL METHOD

The results of the flow simulations presented here were calculated with the RPMTurbo LUFT code. The code is capable of performing steady-state flow simulations and linearized unsteady flow simulations. The partial derivatives required by the linear flow solver are calculated numerically. The code has been validated for flutter analysis [5–7]. The flow model used by the code is the 3D URANS flow equations with the Spalart and Allmaras turbulence model. The turbulence model is fully linearized for the unsteady flow simulations.

Two fluid models were used: ideal gas and wet-steam. The gas constant was R = 461.52 J/kg.K, the absolute viscosity was 1.1E-5 Pa.s and the ratio of specific heats was 1.11 for the ideal gas simulations. An equilibrium wet-steam gas model has been implemented into RPMTurbo's flow solvers and the wet-steam gas model has been fully linearized [8]. Flow properties such as pressure, temperature, speed of sound and viscosity of wet steam are calculated using formulae from IAPWS [9]. The fluid is treated as a single phase and the motion of droplets is not considered.

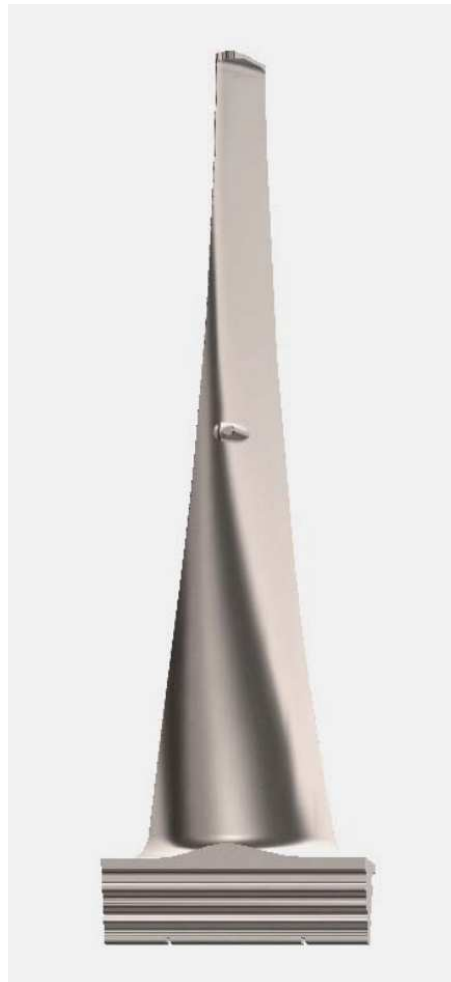

FIGURE 1. LMZ SHROUDED LAST STAGE BLADE

MIXING PLANE

A new feature of the LUFT code is the capability of performing multi-row steady-state simulations with mixing planes. The pitchwise-averaged flow variables at various radial heights are calculated on either side of the mixing plane from the average mass, momentum and total energy in the pitchwise direction. The pitchwise-averaged flow values are interpolated to ghost cells on the other side of the mixing plane. A steady non-reflecting boundary condition is applied either side of the mixing plane.

The mixing plane method was validated by examining the interface between the exit of a steam turbine row and the inlet of the exhaust section. This test case is from an industrial steam turbine similar to one examined later in the paper and at a similar flow condition. The flow domain for the test case is shown in Figure 2. Two inviscid steady-state simulations were performed. The first simulation was a multi-row simulation with separate meshes for the rotating turbine row and the stationary exhaust.

Copyright © 2014 by RPMTurbo & LMZ Power Machines

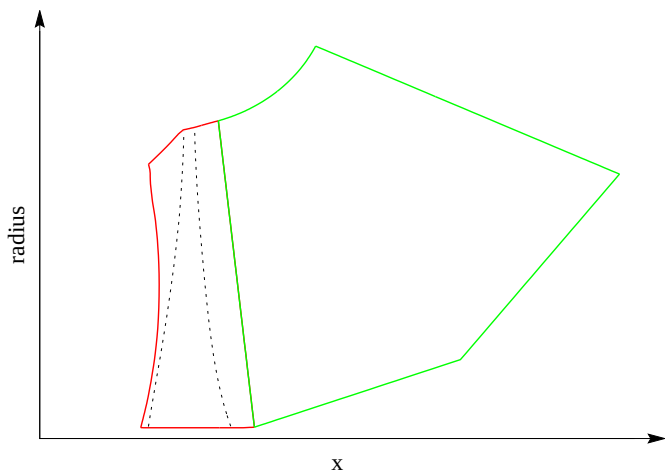

FIGURE 2. SCHEMATIC OF FLOW DOMAINS FOR MIXING PLANE AND NON-REFLECTING BOUNDARY CONDITION TEST CASE

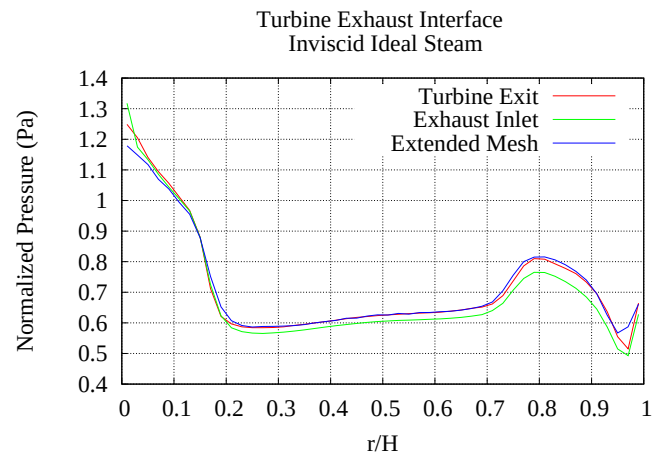

FIGURE 3. PRESSURE AT MIXING PLANE

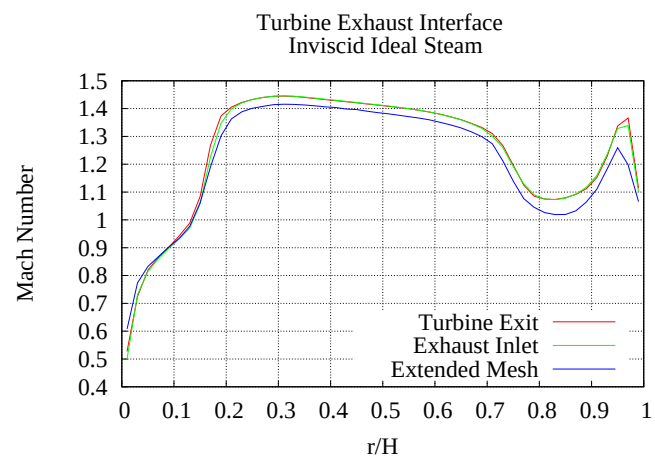

FIGURE 4. MACH NUMBER AT MIXING PLANE

The second simulation used a single mesh for the turbine row and the exhaust section. The exhaust section rotated with the turbine for the second simulation, however, the flow solutions should be equivalent as a slip flow boundary condition (inviscid) was applied at the end walls (hub and shroud).

The pitchwise-averaged flow solutions as a function of radius either side of the mixing plane for the multi-row simulation are compared with the flow solution extracted from the extended mesh at the location of the mixing plane in Figures 3 – 8. The pressure has been normalized by the average pressure applied at the exit of the exhaust section. The flow angles are defined as,

$$\alpha = \tan^{-1}(u_\theta/u_x) \quad (3)$$
$$\beta = \sin^{-1}(u_r/U) \quad (4)$$

where u_x is the axial flow speed, u_θ is the tangential flow speed, u_r is the radial flow speed and $U = \sqrt{(u_x^2 + u_\theta^2 + u_r^2)}$. There is a good agreement between the pressure on the upstream side (turbine exit) of the mixing plane and the pressure extracted from the extended domain (Fig. 3). The pressure on the downstream side of the mixing plane is lower due to the entropy drop caused by averaging the flow in the pitchwise direction. The conservation of energy across the mixing plane is demonstrated in Figure 6. The overall agreement between the flow solution on the upstream side of the mixing plane and the flow solution extracted from the extended mesh suggests that the mixing plane method is working well.

EXACT 3D NON-REFLECTING BOUNDARY CONDITION

Two types of far-field (inlet and outlet) boundary conditions were applied to the unsteady linearized flow simulations: the 3D-NRBC and a one-dimensional non-reflecting boundary condition (1D-NRBC).

The ability of the 3D-NRBC to produce unsteady flow solutions that are independent of the far-field boundary location has been demonstrated previously [7]. However, it was decided to test the application of the 3D-NRBC on an industrial steam turbine case. The test geometry is the same as mixing plane test case (Fig. 2), however, the flow condition was different. The back pressure was higher and the flow at the turbine exit was subsonic (Fig. 9). The flow for this test case was assumed to be inviscid so that the slip wall boundary condition on the ex-

Copyright © 2014 by RPMTurbo & LMZ Power Machines

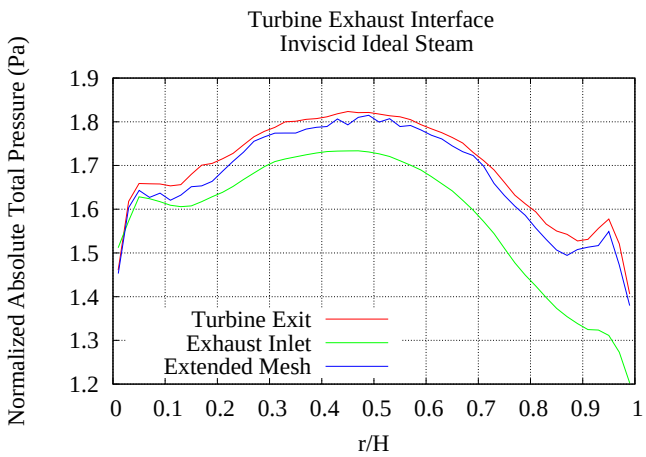

FIGURE 5. TOTAL PRESSURE AT MIXING PLANE

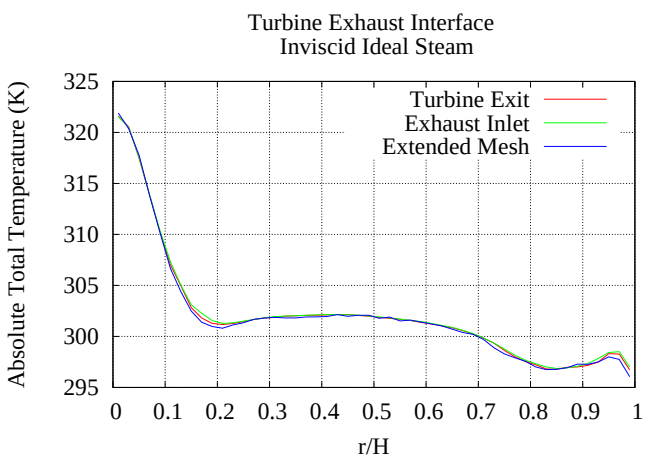

FIGURE 6. TOTAL TEMPERATURE AT MIXING PLANE

haust walls are the equivalent for the extended domain (rotating exhaust) and multi-row (non-rotating exhaust) simulations.

Unsteady linearized flow simulations for a complex traveling wave mode with $n = -15$ were performed on the short turbine domain and on an extended turbine domain which included the exhaust section. Separate simulations applying the 1D-NRBC and the 3D-NRBC were performed for each domain. The calculated normalized work coefficients are shown in Figure 10. There is a significant difference in the work coefficient on the suction side between the solutions calculated with the 1D-NRBC and the 3D-NRBC. This suggests that unsteady flow reflections are occurring at the turbine outlet as the suction surface is facing towards the turbine outlet. The solutions calculated with the 3D-NRBC are independent of the exit location and the solution

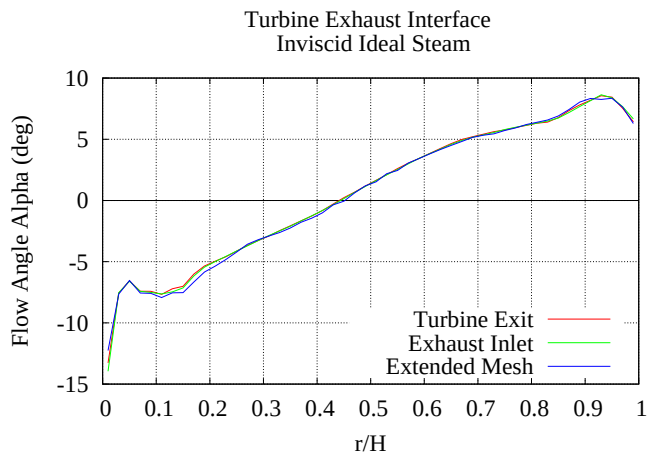

FIGURE 7. ABSOLUTE FLOW ANGLE ALPHA AT MIXING PLANE

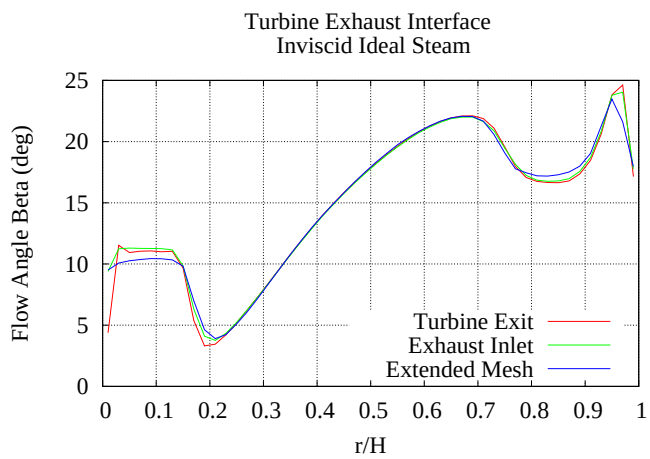

FIGURE 8. ABSOLUTE FLOW ANGLE BETA AT MIXING PLANE

calculated with the 1D-NRBC on the extended domain is closer to the solutions calculated with the 3D-NRBC. This is a good demonstration that the 3D-NRBC is working correctly. These results also suggest that there are no significant unsteady flow wave reflections from the exhaust section back towards the turbine.

The 1D-NRBC assumes that unsteady waves are planar and that the wave fronts are normal to the machine axis. The advantage of the 1D-NRBC is that it is significantly faster than the 3D-NRBC and in some cases the 1D-NRBC gives a similar result to the 3D-NRBC.

Copyright © 2014 by RPMTurbo & LMZ Power Machines

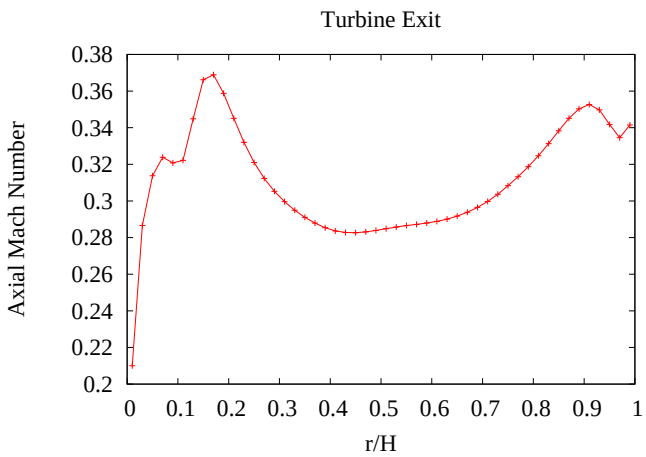

FIGURE 9. AXIAL MACH NUMBER AT TURBINE EXIT FOR NON-REFLECTING BOUNDARY CONDITION TEST CASE

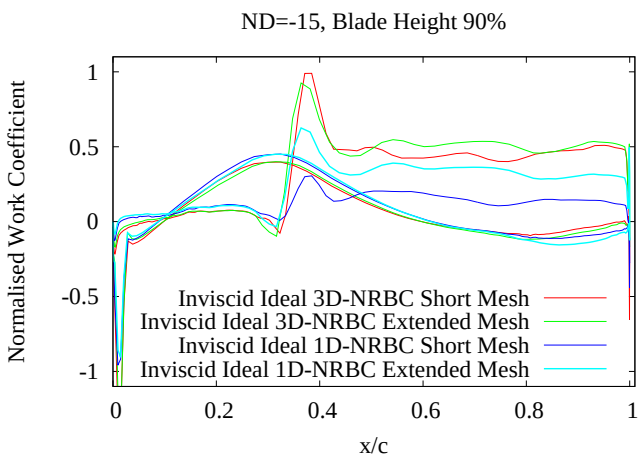

FIGURE 10. TEST NON-REFLECTING BOUNDARY CONDITION AT TURBINE EXIT

STRUCTURAL MODES

The first family of structural modes of the turbine row were considered for the flutter analysis because LMZ has only observed self-excited vibrations for the first family of modes from their measurements. The structural mode shapes were calculated by a FEM method. The contact at the snubber and the tip covers was assumed to be linear with a pair of points either side of the contact surfaces coupled by the symmetry condition. The steady aerodynamic load was not considered. The resulting complex mode shape is shown in Figure 11. The frequencies of the first family of modes normalized by the incoming wake passing frequency are shown in Figure 12.

FIGURE 11. TURBINE BLADE MODE SHAPE FOR NODAL DIAMETER 5

COMPUTATIONAL MODEL

Separate meshes were made for the nozzle, turbine and exhaust section. Multi-block meshes suitable for RANS flow simulations were created for each section. Meshes suitable for inviscid flow simulations were created for the turbine and exhaust section. The height of the first cell on the profile, hub and shroud surfaces were chosen so that the average y^+ would be less than 5.0. An O-mesh was used around the profile. This allows the mesh to be near orthogonal near the profile. This reduces the numerical error in the region near the profile where the flow gradients are high. The meshes were of a high quality with the minimum angle for the turbine meshes greater than 34 degrees. The turbine CFD mesh did not include the snubber and was based on the non-deformed geometry. The details of the meshes are shown in Table 1. Plots of the mesh at the hub and shroud can be seen in Figures 13 and 14 respectively.

For the steady-state simulations, total pressure, total temperature and the flow angles as a function of radius were prescribed at the inlet and an average static pressure was prescribed at the outlet. The incoming turbulent intensity was set to 5.0% for all rows.

Multi-row steady-state simulations of the nozzle row, tur-

Copyright © 2014 by RPMTurbo & LMZ Power Machines

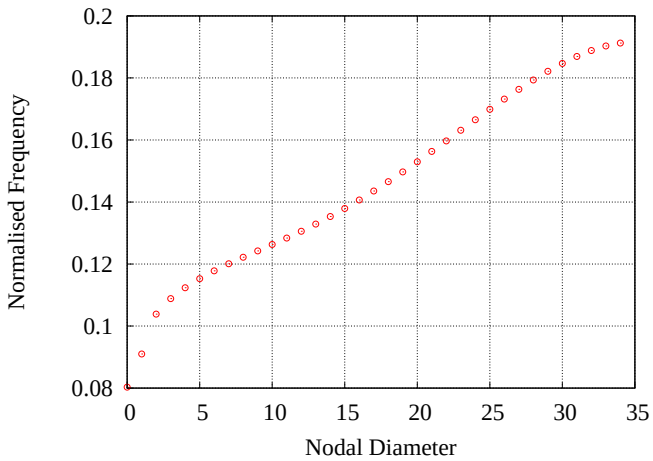

FIGURE 12. MODAL FREQUENCIES NORMALISED BY INCOMING WAKE PASSING FREQUENCY

TABLE 1. DETAILS OF MESHES

Section	Flow	Number Cells	Minimum Angle (degrees)
Nozzle	RANS	763200	24.45
Turbine	RANS	798208	35.44
Exhaust	RANS	24010	69.80
Turbine	Inviscid	543760	34.84
Exhaust	Inviscid	19110	71.19

bine row and exhaust section for the new blade were performed. Mixing planes were used to connect the adjacent rows. A schematic of the flow domain is shown in Figure 15.

GRID MOTION

The motion of the individual grid points of the CFD mesh has to be prescribed before performing the unsteady linearized flow simulations. The grid motion is determined by solving a modified Laplace equation on the CFD mesh. The boundary conditions for the Laplace problem are: the mode shape is interpolated on to the CFD mesh of the profile, zero motion at the inlet, outlet and periodic boundaries and zero normal displacement at the hub and shroud (points can slide). The calculated real and imaginary components of the grid motion in the axial direction for $n = 15$ are shown in Figures 16 and 17. The amplitude of the grid motion used in linear flutter analysis is arbitrary as the calculated logarithmic decrement value is independent of the mode amplitude.

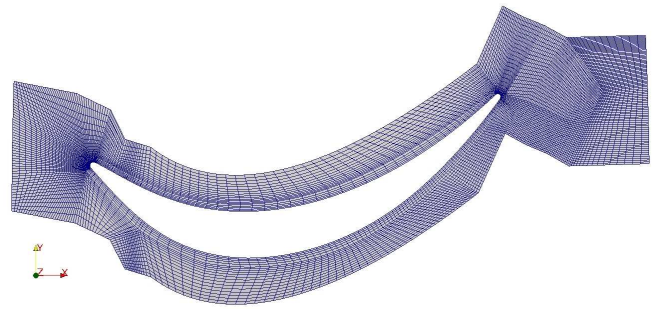

FIGURE 13. TURBINE MESH AT HUB FOR INVISCID FLOW

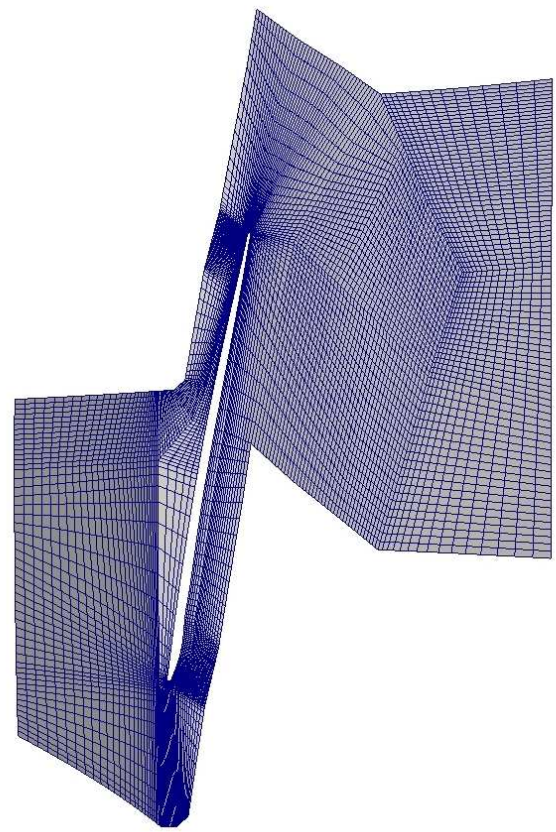

FIGURE 14. TURBINE MESH AT SHROUD FOR INVISCID FLOW

Copyright © 2014 by RPMTurbo & LMZ Power Machines

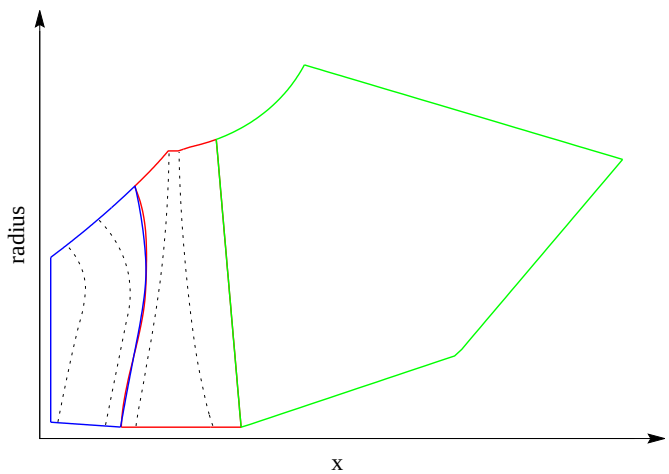

FIGURE 15. SCHEMATIC OF MULTI-ROW FLOW DOMAIN FOR THE NEW BLADE

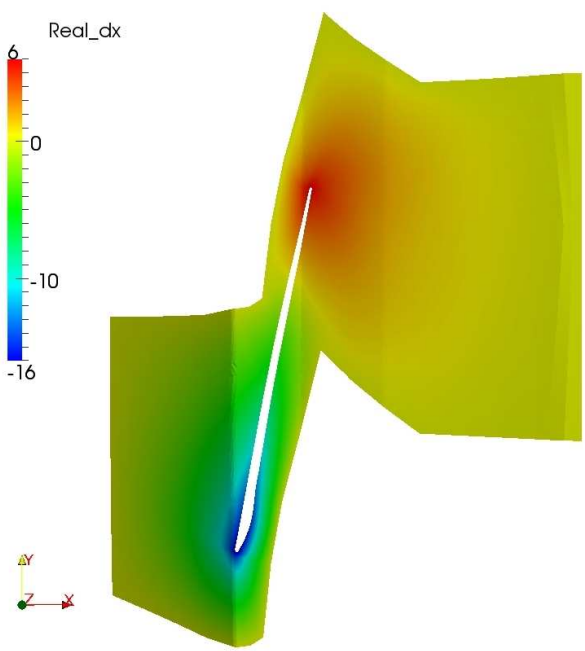

FIGURE 16. REAL GRID MOTION IN AXIAL DIRECTION AT 90% SPAN FOR NODAL DIAMETER 15

STEADY-STATE RESULTS

Steady-state simulations were performed using four different flow models as shown in Table 2. The RANS wet-steam simulation was calculated with the nozzle row, turbine row and exhaust section. The steady-state simulations for the other flow models included the turbine row and the exhaust section. The pitchwise-averaged flow at the turbine inlet predicted by the RANS wet-steam steady simulation was prescribed at the turbine inlet for the steady-state simulations of the other flow models. The Reynolds number of the flow was 340 000, based on the turbine exit flow conditions and the average chord length.

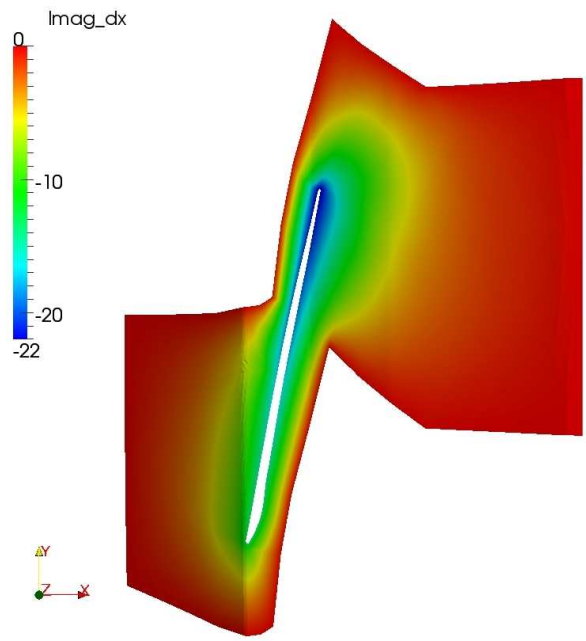

FIGURE 17. IMAGINARY GRID MOTION IN AXIAL DIRECTION AT 90% SPAN FOR NODAL DIAMETER 15

TABLE 2. DETAILS OF STEADY-STATE SIMULATIONS

Flow Equations	Gas Model	Nozzle Included	Mass Flow
RANS	Wet-Steam	yes	1.0
RANS	Ideal	no	1.027
Inviscid	Wet-Steam	no	1.035
Inviscid	Ideal	no	1.015

The calculated flow at the outlet of the turbine domain is mostly supersonic. This can be seen by the fact that the axial Mach number is greater than 1.0 (Fig. 18). This shows the value of including the exhaust section in the steady-state calculation. As the flow at the turbine outlet is mixed subsonic and supersonic (mostly supersonic), it is not possible to apply a steady bound-

Copyright © 2014 by RPMTurbo & LMZ Power Machines

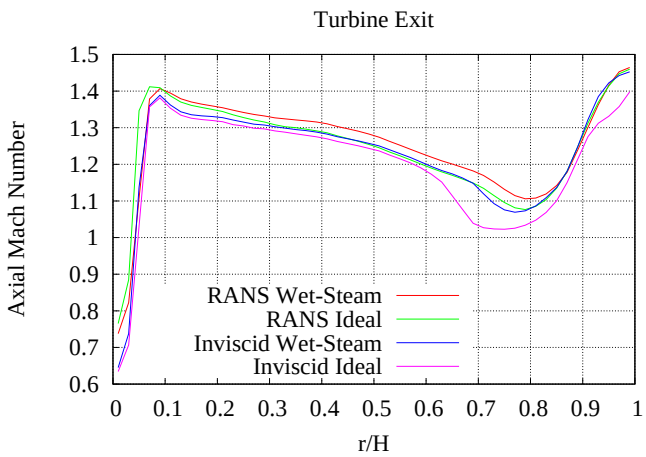

FIGURE 18. ABSOLUTE AXIAL MACH NUMBER AT TURBINE EXIT PREDICTED BY VARIOUS FLOW MODELS

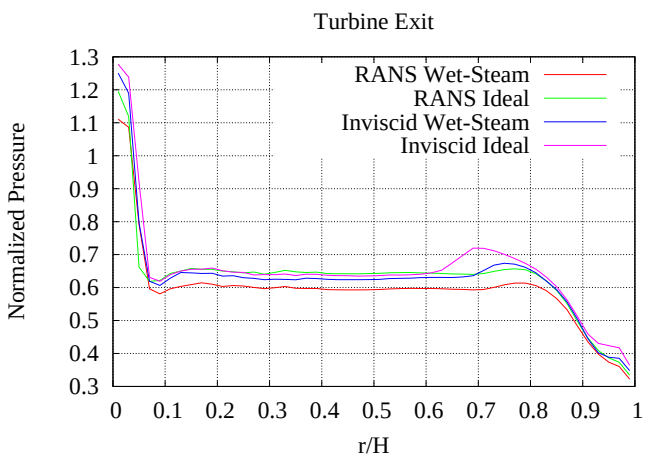

FIGURE 19. NORMALIZED STATIC PRESSURE AT TURBINE EXIT PREDICTED BY VARIOUS FLOW MODELS

ary condition to this boundary without knowing the nature of the flow at various sections of the boundary, as different boundary conditions need to be applied for subsonic and supersonic flow. The flow Mach number in the exhaust section predicted by the RANS wet-steam calculation is shown in Figure 20. It can be seen that the supersonic flow extends well into the exhaust section.

The pressure calculated at the turbine outlet is significantly lower than the pressure prescribed at the outlet of the exhaust section (Fig. 19). The differences in the pressure on the profile at 90% blade height calculated by the different flow models are shown in Figure 21.

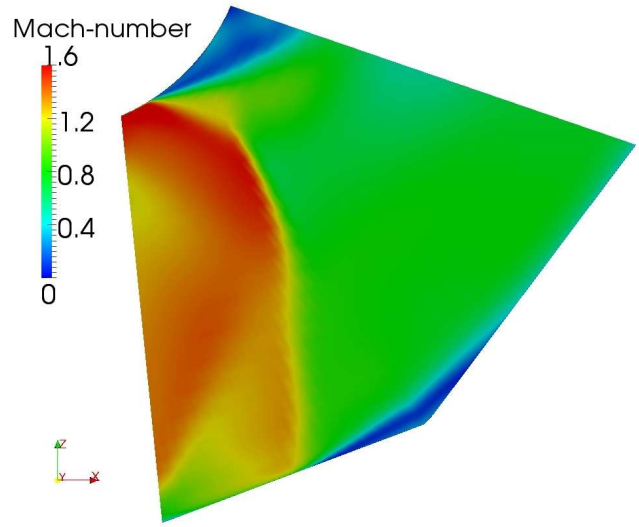

FIGURE 20. FLOW MACH NUMBER IN EXHAUST SECTION PREDICTED BY RANS WET-STEAM SIMULATION

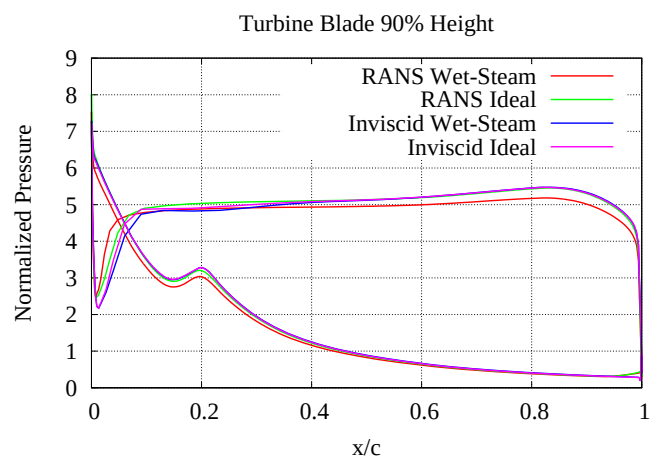

FIGURE 21. NORMALIZED PRESSURE ON PROFILE AT 90% BLADE HEIGHT

UNSTEADY FLOW RESULTS

Linearized flow simulations were performed to calculate the unsteady flow response from the various traveling wave modes. The normalized work performed by the unsteady flow predicted by the various flow models on the pressure and the suction side for the mode corresponding to $n = -15$ are shown in Figures 22 and 23 respectively. Positive values of work coefficient indicate that the aerodynamic forces are adding energy to the blade and hence are unstable. The reduced frequency for $n = -15$ based

Copyright © 2014 by RPMTurbo & LMZ Power Machines

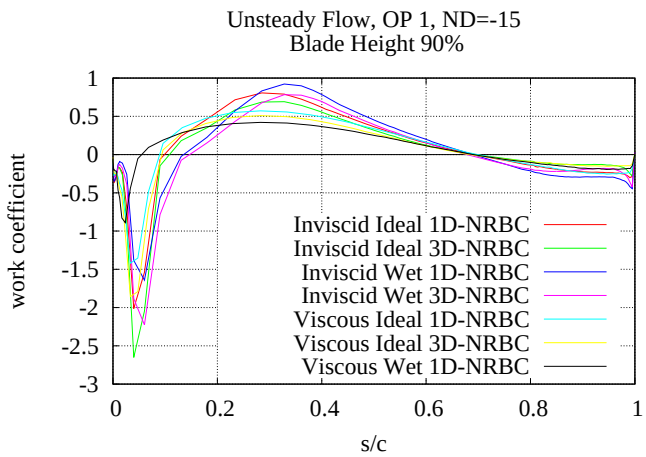

FIGURE 22. NORMALIZED WORK COEFFICIENT ON PRESSURE SIDE AT 90% BLADE HEIGHT FOR NODAL DIAMETER -15

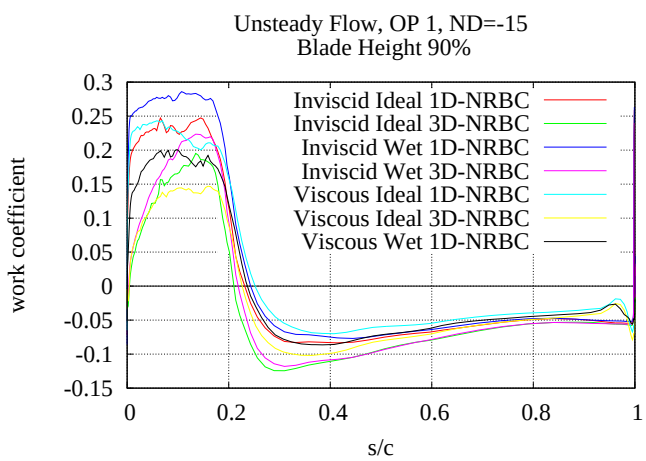

FIGURE 23. NORMALIZED WORK COEFFICIENT ON SUCTION SIDE AT 90% BLADE HEIGHT FOR NODAL DIAMETER -15

on full chord is $\omega^* = 0.363$.

Unfortunately, it was not possible to calculate an unsteady solution for the URANS flow model with wet-steam and the 3D-NRBC. The solution failed to converge. It appears that including all the modeling features makes the linear flow equations for this case too stiff for the linear solver to reduce the residual of the linear problem to an acceptable level. However, it was possible to achieve solutions for all other combinations of flow model, gas model and boundary condition. The work coefficient curves are similar for the various flow models and it is expected that the URANS flow model with the wet-steam gas model and 3D-NRBC would not be significantly different to the other results.

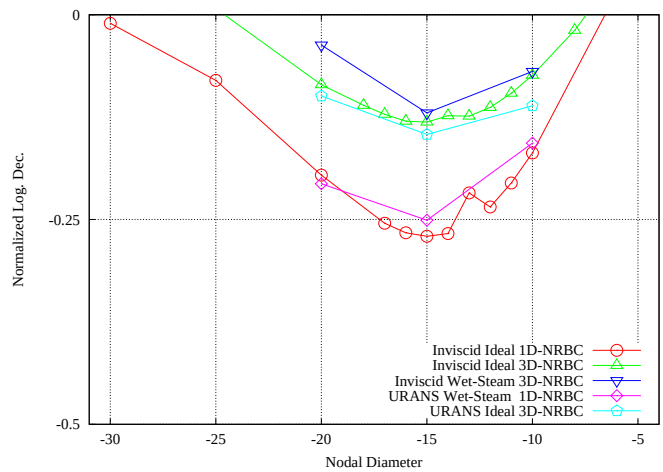

FIGURE 24. PLOT OF NORMALIZED LOGARITHMIC DECREMENT FOR VARIOUS FLOW MODELS

The plot of normalized logarithmic decrement (log.-dec.) versus nodal diameter of the traveling wave modes is shown in Figure 24. Negative aerodynamic damping values are unstable. The log.-dec values are normalized by the magnitude of the minimum log.-dec. value from a similar blade with a known safe working history. The points of the log.-dec. curve were calculated for various flow models. The curves have a similar shape and the least stable mode occurs at $n = -15$ for all models. The modeling feature that causes the biggest difference in the calculated log.-dec. is the choice of the far-field boundary condition. The minimum normalized log.-dec. value for Inviscid Ideal 3D-NRBC is -0.131 compared with -0.270 for Inviscid Ideal 1D-NRBC. The differences in the calculated log.-dec. due to choice of gas model (ideal versus wet-steam) and flow equations (inviscid versus URANS) are small.

The minimum normalized log.-dec. value shown in Figure 24 is -0.27. This suggests that the new blade at this condition should not experience unfavorable flutter vibrations. However, the amount of mechanical damping is dependent on the nodal diameter so the normalized log.-dec. value can not be used as the sole flutter criteria. It is important to compare the log.-dec. value with the expected mechanical damping at the given nodal diameter.

DISCUSSION

The decision to perform a multi-row steady-state calculation with the exhaust section was vindicated because the predicted flow at the turbine exit was mainly supersonic and extended well into the exhaust section. It is not possible to apply a steady boundary condition at the turbine exit if it is not known

Copyright © 2014 by RPMTurbo & LMZ Power Machines

beforehand what regions are subsonic and supersonic.

There were some differences in the work coefficient predicted by inviscid and URANS flow simulations, particularly on the first half of the pressure side (Fig. 22). However, these differences tended to cancel each other out when the logarithmic decrement was calculated for the case examined. If there was a significant region of separated flow then it is expected that the URANS results would differ from the inviscid results and be more accurate.

There were also some differences in the work coefficient predicted by the ideal gas and wet-steam flow simulations on the first half of the pressure side. Once again, these differences tended to cancel each other out when the logarithmic decrement was calculated. Most of the flow through the turbine is a saturated mixture of steam and water droplets. There are only small pockets of superheated vapor immediately downstream of the trailing edge. The isentropic polytropic index of the flow varied from 1.105 to 1.125. It has been shown that if most of the flow is a saturated mixture and the polytropic index is reasonably constant then ideal gas simulations can give similar results to wet-steam calculations [8]. Wet-steam effects may be more important in earlier stages of a steam turbine where condensation first occurs. In this case, the flow will contain regions of superheated steam vapor and regions with saturated flow. The polytropic index of the flow in these different regions would be significantly different and it is expected that the predictions from a wet-steam model would probably be different from the ideal gas predictions.

The application of the 3D-NRBC only made a small change to the unsteady flow solutions for the operating condition examined for the new turbine blade. The flow at the outlet is mostly supersonic so it is not possible for unsteady flow reflections at the outlet to travel upstream and affect the unsteady pressure on the profile. However, there remains the possibility of unsteady flow reflections from the upstream blade row. The outgoing acoustic modes at the inlet are cut-off (decaying) for most of the aeroelastic modes ($|n| < 4$). If there were unsteady flow reflections at the inlet for $n = -15$, the amplitudes of the reflected waves when they return to the blade would be small and would not affect the solution significantly. This is why there is only a small difference between the solutions calculated with the 1D-NRBC and 3D-NRBC. Further work is planned to quantify the influence of unsteady wave reflections from the upstream blade row.

However, the application of the 3D-NRBC did change the unsteady flow solution for the test case shown in Figure 10 where the exhaust pressure is higher. The flow at the turbine exit is subsonic and the down-stream traveling acoustic waves at the outlet are not decaying (cut-on), so it is possible for reflected waves at the outlet to travel upstream and change the work done on the blade.

Unfortunately the authors do not have access to unsteady pressure measurements on steam turbine blade surfaces due to vibrating blades. These measurements would be helpfully to further validate the method. There are some characteristics of the flutter analysis of the last stage steam turbine blade that are not tested by the standard flutter test cases, such as high exit Mach number, high stagger angle and wet-steam flow. The development of new open test cases that examine these characteristics are recommended for future work.

CONCLUSIONS

A flutter analysis of a new steam turbine blade has been presented. The logarithmic decrements of the aeroelastic modes were calculated and compared with a reference case for a similar steam turbine blade, at a condition known to have a long and safe working history. The new steam turbine at the flow condition examined was found to be more stable than the reference case.

The logarithmic decrement values were calculated from the unsteady work predicted by linearized flow simulations. The linearized flow simulations included many advanced features such as URANS flow modeling, a wet-steam equation of state and a three-dimensional non-reflecting boundary condition. Another feature of the flutter analysis was that multi-row steady-state simulations that included the exhaust section were performed. The multi-row steady-state simulations were necessary to accurately predict the flow conditions at the turbine exit, which was mostly supersonic.

ACKNOWLEDGMENT

The simulations reported in this paper were performed using a computer cluster at the High Performance Computing (HPC) facility at the University of Queensland. The authors would like to thank the University of Queensland, the Queensland Cyber Infrastructure Foundation Ltd., the National Computational Infrastructure Specialised Facilities Program, the CSIRO through its partnership in the NCI SF (Bioinformatics) and the EMBL Australia EBI Mirror Project for sponsoring the HPC facility.

REFERENCES

[1] Rice, T., Bell, D., and Singh, G., 2009. “Identification of the Stabiliy Margin Between Safe Operation and the Onset of Blade Flutter”. *Journal of Turbomachinery,* ***131***(1), January, pp. 1–10.

[2] Stüer, H., Schmitt, S., and Ashcroft, G., 2008. “Aerodynamic mistuning of structurally coupled blades”. Proceedings of ASME Turbo Expo 2008: Power for Land, Sea and Air, ASME. GT2008-50204.

[3] Masserey, P.-A., McBean, I., and Lorini, H., 2012. “Analysis and improvement of vibrational behaviour on the ND37 A last stage blade”. *VGB Power Tech Journal*(8).

Copyright © 2014 by RPMTurbo & LMZ Power Machines

[4] Huang, X. Q., He, L., and Bell, D. L., 2006. "Influence of upstream stator on the rotor flutter stability in a low pressure steam turbine stage". In Proc. IMechE Vol. 220 Part A: J. Power and Energy.

[5] Petrie-Repar, P. J., McGhee, A. M., and Jacobs, P. A., 2007. "Three-dimensional viscous flutter analysis of standard configuration 10". In Proceedings of ASME TURBO EXPO. GT2007-27800.

[6] Petrie-Repar, P. J., McGhee, A. M., Jacobs, P. A., and Gollan, R., 2006. "Analytical maps of aerodynamic damping as a function of operating condition for a compressor profile". In Proceedings of ASME TURBO EXPO. GT2006-90829.

[7] Petrie-Repar, P. J., 2010. "Three-dimensional non-reflecting boundary condition for linearized flow solvers". In Proceedings of ASME TURBO EXPO. GT2010-23335.

[8] Petrie-Repar, P. J., 2012. "Establishment of a steam turbine flutter test case". In Proceedings of 13th International Symposium on Unsteady Aerodynamics, Aeroacosutics and Aeroelasticity of Turbomachinery.

[9] Dooley, R. B., 1997. Release on the IAPWS industrial formulation 1997 for the thermodynamic properties of water and steam. Tech. rep., The International Association for the Properties of Water and Steam, Erlangen, Germany.

Copyright © 2014 by RPMTurbo & LMZ Power Machines